Quadratic to linear magnetoresistance tuning in TmB$_4$

Sreemanta Mitra,[1,*] Jeremy Goh Swee Kang,[1] John Shin,[2] Jin Quan Ng,[1] Sai Swaroop Sunku,[1,†] Tai Kong,[3,‡]
Paul C. Canfield,[3] B. Sriram Shastry,[2] Pinaki Sengupta,[1] and Christos Panagopoulos[1,§]

[1]*Division of Physics and Applied Physics, School of Physical and Mathematical Sciences, Nanyang Technological University,
21, Nanyang Link 637371, Singapore*
[2]*Department of Physics, University of California, Santa Cruz, California 95064, USA*
[3]*Ames Laboratory, U.S. DOE and Department of Physics and Astronomy, Iowa State University, Ames, Iowa 50011, USA*

The change of a material's electrical resistance (R) in response to an external magnetic field (B) provides subtle information for the characterization of its electronic properties and has found applications in sensor and storage related technologies. In good metals, Boltzmann's theory predicts a quadratic growth in magnetoresistance (MR) at low B and saturation at high fields. On the other hand, a number of nonmagnetic materials with weak electronic correlation and low carrier concentration for metallicity, such as inhomogeneous conductors, semimetals, narrow gap semiconductors and topological insulators, and two dimensional electron gas, show positive, nonsaturating linear magnetoresistance (LMR). However, observation of LMR in single crystals of a good metal is rare. Here we present low-temperature, angle-dependent magnetotransport in single crystals of the antiferromagnetic metal, TmB$_4$. We observe large, positive, and anisotropic MR(B), which can be tuned from quadratic to linear by changing the direction of the applied field. In view of the fact that isotropic, single crystalline metals with large Fermi surface (FS) are not expected to exhibit LMR, we attribute our observations to the anisotropic FS topology of TmB$_4$. Furthermore, the linear MR is found to be temperature independent, suggestive of quantum mechanical origin.

I. INTRODUCTION

Interest in novel magnetotransport phenomena in metallic magnets is driven by technological and fundamental considerations. The technological motivation comes from harnessing the unique functionalities associated with properties such as giant magnetoresistance, while the fundamental motivation arises from discovering and understanding new quantum many body physics. The quest for linear magnetoresistance (LMR) in strongly correlated systems is one such example of fundamental motivation [1]. Boltzmann's classical electronic transport theory shows that in a conductor with a large Fermi surface (FS), magnetoresistance (MR) [defined as $\frac{\Delta\rho(B)}{\rho(0)} = \frac{\rho(B)-\rho(0)}{\rho(0)}$, where $\rho(B)$ is resistivity in magnetic field B] grows as B^2 at small fields and saturates to a constant value at higher fields [2]. A linear and nonsaturating dependence on B denotes a departure from conventional behavior. Notably, LMR has been found to arise from multiple factors ranging from classical [3–10] to quantum [11,12]. Discovery and understanding of LMR in new materials and controlling the underlying mechanism remains an active research frontier [1,3–26].

The superlinear, nonsaturating MR observed in nonstoichiometric silver chalcogenides [13] (Ag$_{2+\delta}$Se, Ag$_{2+\delta}$Te), two dimensional electron gas (2DEG) [23], and Bi$_2$Se$_3$ [5] were explained using a classical random-resistor model [3,4]. Mobility (μ) [7] and density [10] fluctuations, along with space-charge effect [24], have also been discussed to be the primary origin of LMR in several materials. On the other hand, LMR in single crystals of semimetals [15,16,19], narrow gap semiconductors [20], topological insulators [21,22], and pressure-induced superconductors [1] have been explained with a quantum picture [11,12]. In single crystalline metals with parabolic dispersion, LMR is atypical and only observed previously in some members of the light rare-earth diantimonide (RSb$_2$) and RAgSb$_2$ (R = La-Nd,Sm) families [27,28]. Hence it would be interesting to explore a metal where not only expected quadratic MR is realized, but also a tuning to LMR can be achieved by changing certain experimental parameters, while maintaining the purity and stoichiometry of the single crystal.

We performed low temperature (T), angle-dependent MR measurements on single crystalline TmB$_4$, which belongs to the rare-earth tetraboride family and crystallizes in a tetragonal structure with space group $P4/mbm$, 127. The typical layered crystal structure of TmB$_4$, with four unit cells along the c axis, is shown in Fig. 1(a). Tm atoms lie in the crystalline ab plane, arranged in a Shastry-Sutherland lattice structure [29–31] with approximately equal bond lengths [Fig. 1(b)]. Halfway between the Tm layers, planes of boron atoms form a mixture of four-atom squares and seven-atom rings [31]. There are two different types of boron sites in these planes. One type is an exclusive part of the boron plane, whereas the
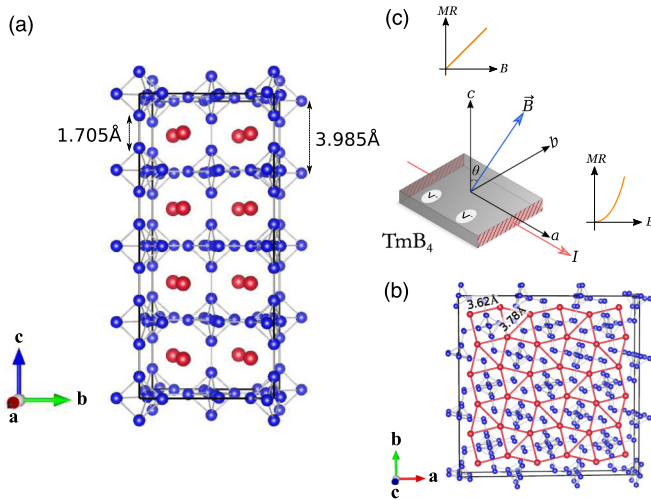
FIG. 1. Structural and experimental considerations. (a) The alternating-layer crystal structure of TmB_4. Four unit cells stacked along the c axis are shown. The Tm (red) atom planes lie halfway between the B (blue) atom layers, which are separated by a distance of 3.985 Å. One type of boron lies exclusively within the boron plane, whereas the other type is part of the boron plane and an octahedral chain along the c axis. (b) A unit cell of TmB_4 viewed along the c axis. The sublattice of Tm atoms maps to a topologically equivalent Shastry-Sutherland lattice structure [29] with perfect squares and nearly equilateral triangles of sides 3.62 Å and 3.78 Å, respectively. The crystal structure of TmB_4 is prepared using VESTA [32]. (c) A schematic of the experimental arrangement and main results. θ is the tilt angle between B and the crystal c axis. The excitation current I is applied parallel to the ab plane of the crystal, indicated in red, while the voltage drop is measured across the two voltage contacts, V^+ and V^-. The MR(B) is linear for $\theta = 0°$ and tunable to quadratic for $\theta = 90°$.

other is part of the boron plane and an octahedral chain along the c axis [31]. Thus the crystal structure has both 2D and 3D features.

The low-temperature magnetic measurements carried out earlier [33–36] on TmB_4 revealed a rich phase diagram with multiple ground states for B applied along the c axis. The ground state is antiferromagnetic (AFM), up to $T = 9.9$ K (for $B = 0$ T) and $B = 1.4$ T (for $T \leqslant 8$ K). At higher values of B and T, the system evolves to various other magnetic ground states, viz. a narrow fractional plateau phase (FPP), a wide half plateau phase, a modulated phase, and a high-field paramagnetic phase [33–36]. Recently, specific heat measurements described FPP not as a distinct thermodynamic ground state of TmB_4, but rather as being degenerate with the AFM phase [37]. Understanding of the various magnetic ground states in TmB_4 has been at the forefront of extensive experimental and theoretical research [33–42], although transport properties [34,36,42] are relatively less studied. Our previous magnetotransport investigation [36] revealed huge, nonsaturating, and hysteretic in-plane MR (900% at 7 T for 2 K) with signatures of unconventional anomalous Hall effect [36]. The large MR along with negative Hall coefficient suggest [36,43] that the carriers have high electronic $\mu \sim 2.9 \, m^2 V^{-1} s^{-1}$ at 2 K.

II. EXPERIMENTAL

Here, we focus on angle-dependent low-temperature magnetotransport experiments in TmB_4 in its AFM phase ($B \leqslant 1.3$ T and $T \leqslant 5$ K). A schematic of the experimental arrangement and the main result of this work are shown in Fig. 1(c), where θ is the tilt angle between B and c axis. We find an unexpected linear MR, tunable to quadratic by varying θ. Single crystals of TmB_4 were grown in a solution growth method using Al solution. Details of the crystal growth can be found elsewhere [35]. For MR measurements, the crystal was oriented [36] and cut into pieces with its faces along (001) direction using a tungsten wire. A rectangular piece of dimensions ~ 0.434 mm $\times 0.516$ mm $\times 0.226$ mm (weighing ~ 0.35 mg) has been used for the measurements. The measurement was done in a standard four point probe method using a Quantum Design Physical Property Measurement System (PPMS). The contacts were made with electrically conductive silver epoxy paste (EpoTeK E4110) and gold wires of diameter $25 \, \mu m$ and $50 \, \mu m$ as connectors for voltage and current contacts, respectively. All measurements were conducted well within the AFM phase ($B \leqslant 1.3$ T and $T \leqslant 5$ K). The angle-dependent magnetotransport measurements were performed by placing the sample on a precision steeper controlled horizontal rotator puck, which can move around an axis perpendicular to B. The excitation current (1.8 mA and 5.0 mA) was applied parallel to the ab plane and B was applied along various directions, relative to the crystal c axis [see Fig. 1(c)]. The linearity of current voltage was ensured at both 300 K and 2 K prior to the magnetotransport measurements. We found in all cases that the MR is minimum at $B = 0$. The raw data of MR was then symmetrized to reflect the expected B to $-B$ invariance, and is plotted in Fig. 3(a). For the anisotropic magnetoresistance (AMR) measurements, R was measured as the sample was rotated continuously at a fixed B and T.

III. RESULTS AND DISCUSSION

Figure 2 depicts the metallic [36] T dependence of the in-plane resistivity (ρ_{ab}) of TmB_4 in a longitudinal ($B \parallel c$-axis) field with varying field strengths. At room temperature [36], the zero-field resistivity, $\rho_{ab}(B = 0)$, is $5 \times 10^{-7} \, \Omega m$ and decreases monotonically with decreasing T down to $12.9 \times 10^{-9} \, \Omega m$ at 2 K giving residual resistivity ratio ($r_R = \frac{\rho_{300 \, K}}{\rho_{2 \, K}}) = 38$. The r_R value is either comparable to or even slightly higher than the previously studied TmB_4 crystals [34,42], suggesting a good quality crystal with a moderate amount of impurity. At $B = 0$, the ratio of ρ_{ab} to the c-axis resistivity [36], ρ_c, is 0.454 at 2 K. Loss of spin-disorder scattering causes a sudden drop in ρ_{ab} at 11.9 K (at $B = 0$) as the system undergoes a magnetic phase transition from the paramagnetic to the modulated phase. Following this second order phase transition, a first order phase transition appears at 9.9 K ($B = 0$) as the system moves from the magnetically ordered modulated phase to an AFM state. Under B, these transition T's shift to lower values.

As shown in the inset of Fig. 2, zero-field $\frac{d\rho_{ab}}{dT}$ shows maxima at $T = 9.9$ K and 11.9 K, indicative of the above-mentioned phase transitions. For $T \leqslant 9$ K, $\frac{d\rho_{ab}}{dT}$ decreases linearly with decreasing T down to 4 K, implying a T^2 variation
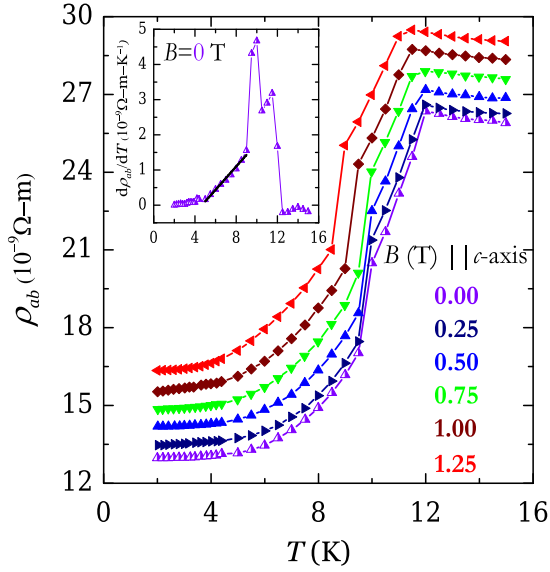
FIG. 2. Temperature and field dependence of electrical resistivity (ρ) in the TmB$_4$ single crystal. Plots of in-plane electrical resistivity (ρ_{ab}), measured in various B, applied parallel to the crystal c axis, against T. At $B = 0$, the transition from the paramagnetic state to the modulated state occurs at 11.9 K and transition from modulated phase to AFM phase occurs at 9.9 K. ρ_{ab} increases and transition temperature decreases as B is increased. For the angle-dependent magnetotransport measurements, we consider the lower part [$2 \leqslant T$ (K) $\leqslant 5$] of the $\rho_{ab} - T$ curve. The lines are to guide the eye. Inset: T derivative of $\rho_{ab}(B = 0)$ against T shows two maxima at the point of inflections of $\rho_{ab} - T$, implying the phase transitions. The abscissa of the inset has the same label as the main panel. The black solid line is the linear fit to the experimental data, signifying a T^2 dependence of ρ_{ab}, in accordance with the Fermi liquid behavior.

of resistivity and is almost T independent in the lower T regime. This T^2 dependence of resistivity at low T, in a metal with magnetic ordering can arise either from $e - e$ scattering or scattering of conduction electrons from magnons [44]. A dominant e-magnon contribution results in a negative MR due to the suppression of magnons [45] under B. However, unlike magnetic metals, TmB$_4$ exhibits a positive MR and ρ_{ab} increases with B (Fig. 2). This rules out scattering from magnons as the primary source of resistivity in TmB$_4$ and only $e - e$ scattering persists in accordance with Fermi liquid theory ($\rho_{ab} = \rho_0 + \beta T^2$, where ρ_0 is the residual resistivity). $\rho_c(T)$ also follows a similar T^2 behavior [36]. The coefficient β is inversely proportional to Fermi temperature and is set by the exponent of T rather than the residual resistivity [46]. While, for the in-plane transport, $\beta = 1.6 \times 10^{-10}$ ΩmK^{-2}, its out-of-plane value is 83×10^{-10} ΩmK^{-2}.

Figure 3(a) shows a set of normalized MR(B) isotherms of TmB$_4$ with $\theta = 0°$ to $90°$, measured at $T = 3$ K. Here, $0°$ ($90°$) refers to a field B applied parallel (perpendicular) to the crystal's c axis [see Fig. 1(c)]. Unexpectedly, for $\theta = 0°$ to $45°$ the MR response is linear all the way down to very small fields. The functional behavior of MR(B) changes gradually to quadratic as $\theta \to 90°$. While the classical MR does not have any response when B is applied parallel to the excitation current, we observed a close to quadratic growth of MR for $B \parallel I \parallel ab$. The change in MR over the B range ($\theta = 90°$) is less than 50% of that observed for $\theta = 0°$. MR ($B = 1.3$ T) is maximum for $\theta = 0°$ ($\approx 25\%$) and minimum ($\approx 10.3\%$) for $\theta = 90°$. MR(B) essentially shows similar features at other temperatures in the AFM phase. One of the notable features of the LMR in TmB$_4$ is that it persists down to lowest applied field, without showing any signature of crossover to a quadratic behavior with change in B, as observed in
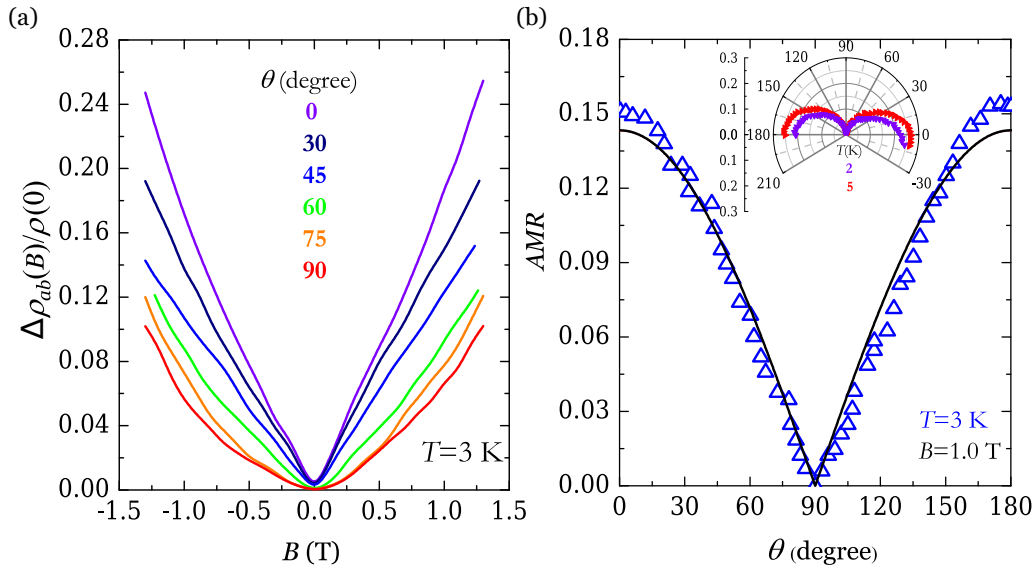

FIG. 3. Angular dependence of MR. (a) A generic MR(B) isotherm measured at $T = 3$ K, under various magnetic field directions. $0°$ ($90°$) refers to whether B is applied parallel (perpendicular) to the crystal's c axis. A linear MR can be seen for $\theta = 0°$, which gradually moves to a quadratic form for $\theta = 90°$. The MR is anisotropic. For $B = 1.3$ T, the MR is $\approx 25\%$ at $\theta = 0°$, whereas it is $\approx 10.3\%$ for $\theta = 90°$. (b) The θ variation of anisotropic magnetoresistance (AMR) (see text) measured at $B = 1.0$ T and $T = 3$ K. The experimental data can be described by a $|\cos\theta|$ function (solid line) indicating a quasi-2D FS [16,19]. Inset: Polar plot of AMR(θ) measured at $T = 2$ K and 5 K, at $B = 1.3$ T. The AMR shows two lobes over the full range of θ, suggesting a twofold symmetry.
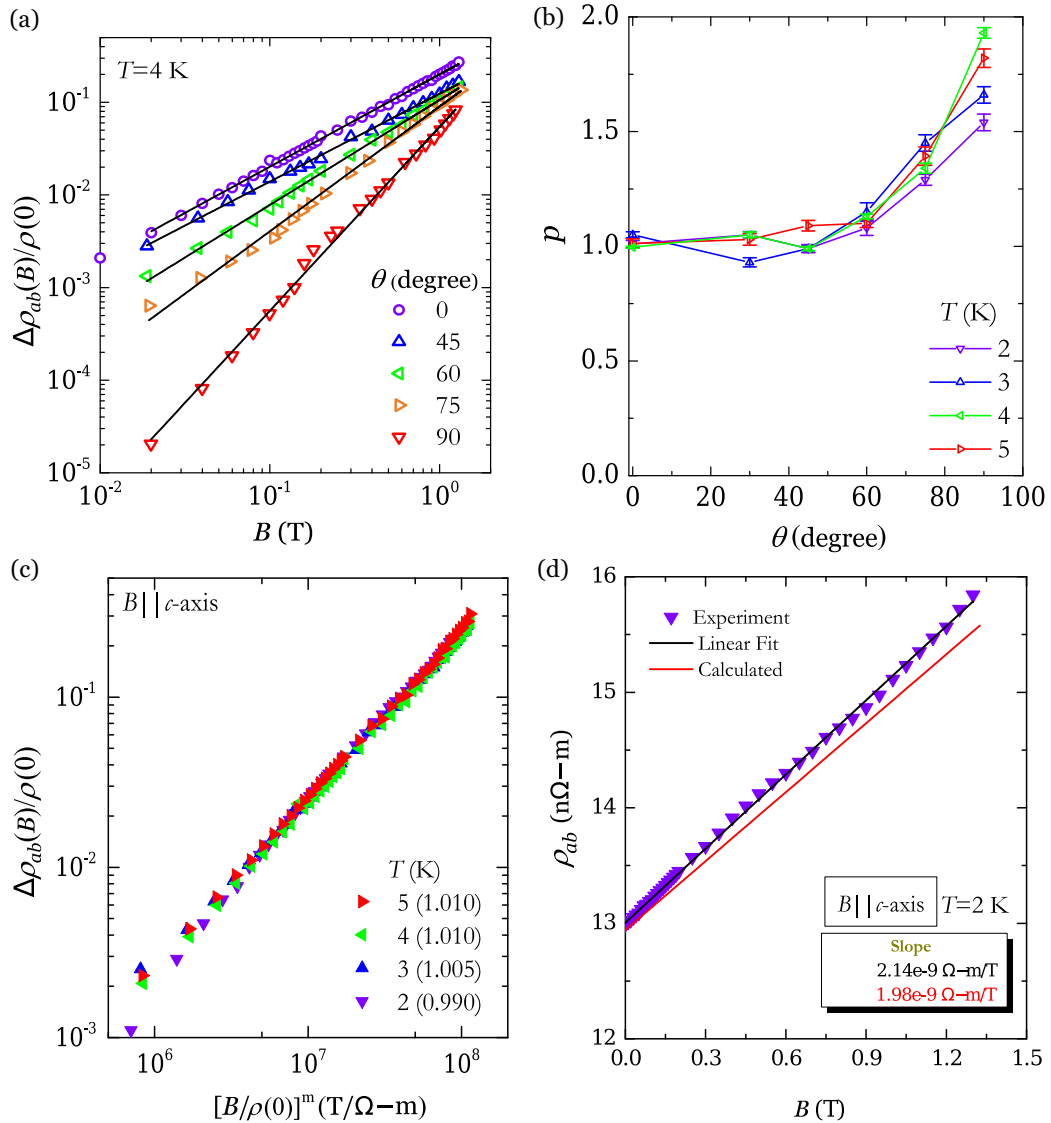
FIG. 4. Analysis of the magnetoresistance data for TmB$_4$. (a) Magnetoresistance isotherm, measured at $T = 4$ K, under five different field orientations, shown in a double logarithmic representation. The linearity in the log-log plot suggests a power law behavior, MR $= (\frac{B}{B_0})^p$. The solid lines are the fit of the experimental data to the power law. (b) The variation of the exponent, p, with θ, for various T's. For $\theta = 0°$, p is close to 1, suggesting linear MR and gradually moves to a value close to 2, for $\theta = 90°$. The error for determining the value of p from the fit (a) is ~0.01 and shown in the plot. p varies in a similar manner for all T's. The lines are to guide the eye. (c) T scaling (Kohler rule) of MR for B along c axis. The values of m used to scale the different T MR data are mentioned in the parentheses. (d) Comparison of the experimental data (violet) and theoretical (red) plot. The experimental data was obtained for $B \parallel c$-axis configuration and measured at $T = 2$ K. The black solid line is the linear fit to the experimental data. The theoretical curve was calculated from Eq. (1) using the values of N_i and n_e (see text). The values of both slopes (inset) agree within 7%.

CaMnBi$_2$ [16], InAs [20], 2DEG [23], and CrAs [1]. Instead, this LMR is similar to the superlinear MR behavior observed in nonstoichiometric silver chalcogenides [13], Bi [14], WTe$_2$ [19], and rare-earth diantimonides [27]. The slope of $\rho_{ab}(B, 0°)$ is $(2.21 \pm 0.01) \times 10^{-9}$ ΩmT^{-1} and almost T independent, suggesting the MR is not due to the phonon scattering [20].

Furthermore, we find MR to be anisotropic. We define anisotropic magnetoresistance [AMR(θ)] as $\frac{R(\theta) - R_{\min}}{R_{\min}}$, where $R(\theta)$ is the resistance at any θ, measured at a constant B and T, and $R_{\min}$ is the minimum resistance obtained as θ is varied. In Fig. 3(b), we show the variation of AMR (θ) at

$T = 3$ K for $B = 1.0$ T. AMR is maximum for $B \parallel c$ axis and diminishes as B is rotated away from the c axis. The data can be satisfactorily fit with a $|\cos \theta|$ dependence. This suggests a (quasi-)2D FS [2,16,19], where MR responds to the perpendicular component of the applied field, $B |\cos \theta|$. The anisotropic MR further suggests an anisotropy in the electronic effective mass [19]. AMR shows twofold symmetry [inset, Fig. 3(b)].

To quantify the evolution of MR from linear to quadratic, we fit MR(B, θ) to $(\frac{B}{B_0})^p$. A representative MR(B) plot (in double logarithmic scale), measured at 4 K for different θ values, is shown in Fig. 4(a). For $\theta = 0°$, $p \cong 1$ and gradually
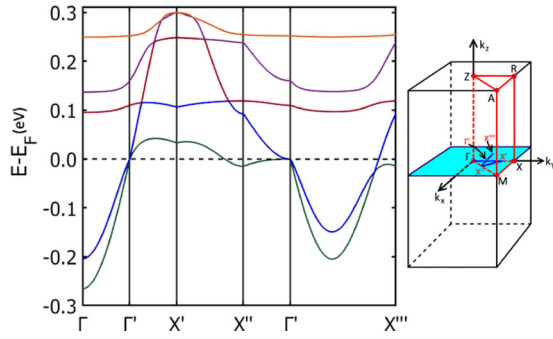
FIG. 5. Band structure for TmB_4 from the spin polarized DFT calculation using the GGA+U method, which shows dispersion in the *ab* plane. The right panel shows the path (in blue) taken in the BZ, Γ-Γ'-X'-X''-Γ'-X'''. A band crossing is observed exactly at E_F with linear dispersion in the $k_x - k_y$ plane at Γ'.

grows to $p \approx 2$ (varies between 1.5 to 1.9, for different T's) for $\theta = 90°$ [Fig. 4(b)]. Crucially, $p(\theta)$ varies similarly at all temperatures and has a negligible T dependence within the AFM phase [Fig. 4(b)].

MR (B, $\theta = 0$) data at different T's can be scaled using the Kohler relation, MR $= \alpha(T)[\frac{B}{\rho(0)}]^m$ [Fig. 4(c)]. The scaling suggests that carriers with single salient relaxation time [2] govern magnetotransport for $B \parallel c$ axis in the AFM phase. Furthermore, this robust T scaling, using a single α, adds credence to the relative T insensitivity of LMR and implies negligible phononic contributions. Therefore, the measured MR is primarily governed by scattering of conduction electrons by impurities.

The origin of LMR in TmB_4 is not entirely clear, but it is plausible that Abrikosov's theory of quantum linear MR [11,12,26,47] can be invoked for this purpose, considering the topology of the FS of TmB_4 [31]. The presence of two symmetry related small pockets (as evident from the spin-polarized DFT calculation using GGA+U method [48]) in the $k_x - k_y$ plane of the Brillouin zone (BZ) along the $\Gamma - X$ direction (labeled Γ' in Fig. 5), with an approximately linear crossing of two bands at the Fermi energy, E_F (within the numerical accuracy) (Fig. 5), is of particular interest here. The low density and small effective mass of the carriers due to the linear band crossing ensure that they can be confined to the lowest Landau level and thus reach the extreme quantum limit even at small (longitudinal) applied fields. This results to a LMR and is given by

$$\rho_{xx} = \frac{N_i B}{\pi c e n_e^2}, \tag{1}$$

provided the carrier concentration (n_e) satisfies $n_e \lesssim (\frac{m_{zz}}{m_{xy}})^{\frac{1}{2}}(\frac{eB}{\hbar c})^{\frac{3}{2}}$ where m_{zz} and m_{xy} are the effective mass of the carriers for motion along k_z and in the $k_x - k_y$ plane, respectively and $N_i (\ll n_e)$ is the density of static scattering centers [11,12,26,47]. The low effective mass of the carriers further gives a T limit for lowest Landau level confinement (see Supplemental Material [49]), which is indeed satisfied in our experiments [50]. At small fields, due to the low effective mass of the electrons from the Fermi pockets, and consequently their high cyclotron frequency, the linear contribution

dominates over the usual quadratic MR from the rest of the FS [47]. Using the values of carrier density and their effective masses estimated from band structure calculations [51], as well as impurity concentrations (see Supplemental Material [49]) from sample preparation conditions, Eq. (1) yields an MR(B) that is in agreement with the experimentally observed magnetotransport data in TmB_4 [Fig. 4(d)]. The compliance of MR (B, $\theta = 0$) to Kohler scaling provides further support to the assumption that magnetotransport at small longitudinal fields is dominated by charge carriers from identical Fermi pockets.

The mechanism identified above explains another intriguing feature of TmB_4—the absence of Shubnikov–de Haas (SdH) oscillations in the observed MR data. Since the extreme quantum limit is already reached at very small fields for the pocket under consideration, there are no Landau level crossings of the FS with increasing field, and consequently no SdH oscillations. In principle, the SdH oscillations should be observed for B along the *ab* plane, but we could not reach the required B, due to strong magnetic fluctuations and experimental limitations.

Finally, the absence of LMR for transverse magnetic fields can also be understood from the anisotropic FS topology. Being a layered material, the small pockets in the $k_x - k_y$ plane of TmB_4 are believed to originate from the overlap of bands close to the FS due to the interlayer coupling. Consequently, there are no such pockets at corresponding points on the surface of the BZ in the *XY* plane. Since magnetotransport of a solid is governed by the external cross section of the FS along the field direction [16], only the quadratic contribution of the total conductivity persists for B applied along the principal plane. This picture, based on the topology of the FS of TmB_4, qualitatively explains the experimental observation of tuning MR from quadratic to linear as the field direction is rotated.

It should be noted that the above discussion is a plausible rather than a rigorous elucidation for the origin of LMR in TmB_4. The present explanation depends crucially on the existence of a linear band crossing very close to the FS in the $k_x - k_y$ plane. Unfortunately, DFT is unable to capture the effects of strong correlations with high accuracy; therefore, one must regard the interpretation as tentative and a much rigorous analytic calculation is indeed required for better insight into the problem. However, it is interesting that the present approach based on anisotropic FS topology within the quantum linear magnetoresistance framework is consistent with the experimental observations. It thus provides a useful platform for further studies of this compelling phenomenon.

IV. SUMMARY

In summary, we have discussed the tuning of MR from linear to quadratic in single crystalline metal, TmB_4, by rotating B relative to the crystal c axis. We give a plausible explanation of the LMR in this metallic system based on its FS topology within the quantum linear magnetoresistance picture, which predominantly holds true for semimetals and topological insulators. We argued that the linear dispersion near E_F and the subsequent Fermi pocket in the FS of TmB_4, arising from its layered structure, give rise to a LMR in an

otherwise normal metal and its complex FS topology governs the tuning of in-plane MR from quadratic to linear.

ACKNOWLEDGMENTS

[1] Q. Niu, W. C. Yu, K. Y. Yip, Z. L. Lim, H. Kotegawa, E. Matsuoka, H. Sugawara, H. Tou, Y. Yanase, and S. K. Goh, Nat. Commun. **8**, 15358 (2017).

[2] A. B. Pippard, *Magnetoresistance in Metals* (Cambridge University Press, Cambridge, UK, 1989), p. 253.

[3] M. M. Parish and P. B. Littlewood, Nature (London) **426**, 162 (2003).

[4] M. M. Parish and P. B. Littlewood, Phys. Rev. B **72**, 094417 (2005).

[5] Y. Yan, L.-X. Wang, D.-P. Yu, and Z.-M. Liao, Appl. Phys. Lett. **103**, 033106 (2013).

[6] P. S. Alekseev, A. P. Dmitriev, I. V. Gornyi, V. Y. Kachorovskii, B. N. Narozhny, M. Schütt, and M. Titov, Phys. Rev. Lett. **114**, 156601 (2015).

[7] A. Narayanan, M. D. Watson, S. F. Blake, N. Bruyant, L. Drigo, Y. L. Chen, D. Prabhakaran, B. Yan, C. Felser, T. Kong, P. C. Canfield, and A. I. Coldea, Phys. Rev. Lett. **114**, 117201 (2015).

[8] J. C. W. Song, G. Refael, and P. A. Lee, Phys. Rev. B **92**, 180204(R) (2015).

[9] F. Kisslinger, C. Ott, and H. B. Weber, Phys. Rev. B **95**, 024204 (2017).

[10] T. Khouri, U. Zeitler, C. Reichl, W. Wegscheider, N. E. Hussey, S. Wiedmann, and J. C. Maan, Phys. Rev. Lett. **117**, 256601 (2016).

[11] A. A. Abrikosov, Sov. Phys. JETP **29**, 746 (1969).

[12] A. A. Abrikosov, Phys. Rev. B **58**, 2788 (1998).

[13] R. Xu, A. Husmann, T. F. Rosenbaum, M.-L. Saboungi, J. E. Enderby, and P. B. Littlewood, Nature (London) **390**, 57 (1997).

[14] F. Y. Yang, K. Liu, K. Hong, D. H. Reich, P. C. Searson, and C. L. Chien, Science **284**, 1335 (1999).

[15] A. L. Friedman, J. L. Tedesco, P. M. Campbell, J. C. Culbertson, E. Aifer, F. K. Perkins, R. L. Myers-Ward, J. K. Hite, C. R. Eddy, G. G. Jernigan, and D. K. Gaskill, Nano Lett. **10**, 3962 (2010).

[16] K. Wang, D. Graf, L. Wang, H. Lei, S. W. Tozer, and C. Petrovic, Phys. Rev. B **85**, 041101(R) (2012).

[17] Y. Kopelevich, R. R. da Silva, B. C. Camargo, and A. S. Alexandrov, J. Phys.: Condens. Matter **25**, 466004 (2013).

[18] T. Liang, Q. Gibson, M. N. Ali, M. Liu, R. J. Cava, and N. P. Ong, Nat. Mater. **14**, 280 (2015).

[19] Y. Zhao, H. Liu, J. Yan, W. An, J. Liu, X. Zhang, H. Wang, Y. Liu, H. Jiang, Q. Li, Y. Wang, X.-Z. Li, D. Mandrus, X. C. Xie, M. Pan, and J. Wang, Phys. Rev. B **92**, 041104(R) (2015).

[20] J. Hu and T. F. Rosenbaum, Nat. Mater. **7**, 697 (2008).

[21] X. Wang, Y. Du, S. Dou, and C. Zhang, Phys. Rev. Lett. **108**, 266806 (2012).

[22] S. Barua, K. P. Rajeev, and A. K. Gupta, J. Phys.: Condens. Matter **27**, 015601 (2014).

[23] M. A. Aamir, S. Goswami, M. Baenninger, V. Tripathi, M. Pepper, I. Farrer, D. A. Ritchie, and A. Ghosh, Phys. Rev. B **86**, 081203(R) (2012).

[24] M. P. Delmo, S. Yamamoto, S. Kasai, T. Ono, and K. Kobayashi, Nature (London) **457**, 1112 (2009).

[25] I. M. Hayes, R. D. McDonald, N. P. Breznay, T. Helm, P. J. W. Moll, A. S. Mark Wartenbe, and J. G. Analytis, Nat. Phys. **12**, 916 (2016).

[26] A. A. Abrikosov, Phys. Rev. B **60**, 4231 (1999).

[27] S. L. Bud'ko, P. C. Canfield, C. H. Mielke, and A. H. Lacerda, Phys. Rev. B **57**, 13624 (1998).

[28] K. D. Myers, S. L. Bud'ko, I. R. Fisher, Z. Islam, H. Kleinke, A. H. Lacerda, and P. C. Canfield, J. Magn. Magn. Mater. **205**, 27 (1999).

[29] B. S. Shastry and B. Sutherland, Physica B+C **108**, 1069 (1981).

[30] S. Michimura, A. Shigekawa, F. Iga, T. Takabatake, and K. Ohoyama, J. Phys. Soc. Jpn. **78**, 024707 (2009).

[31] J. Shin, Z. Schlesinger, and B. S. Shastry, Phys. Rev. B **95**, 205140 (2017).

[32] K. Momma and F. Izumi, J. Appl. Crystallogr. **44**, 1272 (2011).

[33] K. Siemensmeyer, E. Wulf, H.-J. Mikeska, K. Flachbart, S. Gabáni, S. Mat'aš, P. Priputen, A. Efdokimova, and N. Shitsevalova, Phys. Rev. Lett. **101**, 177201 (2008).

[34] S. Gabáni, S. Mat'aš, P. Priputen, K. Flachbart, K. Siemensmeyer, E. Wulf, A. Evdokimova, and N. Shitsevalova, Acta Phys. Pol. A **113**, 227 (2008).

[35] K. Wierschem, S. S. Sunku, T. Kong, T. Ito, P. C. Canfield, C. Panagopoulos, and P. Sengupta, Phys. Rev. B **92**, 214433 (2015).

[36] S. S. Sunku, T. Kong, T. Ito, P. C. Canfield, B. S. Shastry, P. Sengupta, and C. Panagopoulos, Phys. Rev. B **93**, 174408 (2016).

[37] J. Trinh, S. Mitra, C. Panagopoulos, T. Kong, P. C. Canfield, and A. P. Ramirez, Phys. Rev. Lett. **121**, 167203 (2018).

[38] Z. Fisk, M. B. Maple, D. C. Johnston, and L. D. Woolf, Solid State Commun. **39**, 1189 (1981).

[39] S. Yoshii, T. Yamamoto, M. Hagiwara, A. Shigekawa, S. Michimura, F. Iga, T. Takabatake, and K. Kindo, J. Phys.: Conf. Ser. **51**, 59 (2006).

[40] T. Suzuki, Y. Tomita, N. Kawashima, and P. Sengupta, Phys. Rev. B **82**, 214404 (2010).

[41] Y. I. Dublenych, Phys. Rev. Lett. **109**, 167202 (2012).

[42] L. Ye, T. Suzuki, and J. G. Checkelsky, Phys. Rev. B **95**, 174405 (2017).

[43] C. Shekhar, A. K. Nayak, Y. Sun, M. Schmidt, M. Nicklas, I. Leermakers, U. Zeitler, Y. Skourski, J. Wosnitza, Z. Liu,

Y. Chen, W. Schnelle, H. Borrmann, Y. Grin, C. Felser, and B. Yan, Nat. Phys. **11**, 645 (2015).

[44] D. A. Goodings, Phys. Rev. **132**, 542 (1963).

[45] P. V. P. Madduri and S. N. Kaul, Phys. Rev. B **95**, 184402 (2017).

[46] X. Lin, B. Fauqué, and K. Behnia, Science **349**, 945 (2015).

[47] A. A. Abrikosov, Europhys. Lett. **49**, 789 (2000).

[48] For calculation details, please see Ref. [31].

[49] See Supplemental Material at http://link.aps.org/supplemental/10.1103/PhysRevB.99.045119 for details on the following: A comparison between the residual resistivity (RR) of our sample and similarly grown TmB_4 crystals with known impurity density [52] allows us to estimate N_i (assuming the RR arises solely from scattering of electrons off impurity), as 10^{21} m^{-3}.

[50] Above this T value, we previously observed a quadratic MR for $B \parallel c$ axis. Please see Ref. [36] for details.

[51] Estimating n_e^{pocket} is tricky, since the pocket is reduced to a point in the zero-field first principle calculations. However, as a rough estimate, we can use the calculated value for the other smallest Fermi pockets [31], viz., $n_e(\sim 10^{24}$ m$^{-3})$.

[52] S. Okada, K. Kudou, Y. Yu, and T. Lundström, Jpn. J. Appl. Phys **33**, 2663 (1994).